

# PCCP

Accepted Manuscript



This is an *Accepted Manuscript*, which has been through the Royal Society of Chemistry peer review process and has been accepted for publication.

*Accepted Manuscripts* are published online shortly after acceptance, before technical editing, formatting and proof reading. Using this free service, authors can make their results available to the community, in citable form, before we publish the edited article. We will replace this *Accepted Manuscript* with the edited and formatted *Advance Article* as soon as it is available.

You can find more information about *Accepted Manuscripts* in the [Information for Authors](#).

Please note that technical editing may introduce minor changes to the text and/or graphics, which may alter content. The journal's standard [Terms & Conditions](#) and the [Ethical guidelines](#) still apply. In no event shall the Royal Society of Chemistry be held responsible for any errors or omissions in this *Accepted Manuscript* or any consequences arising from the use of any information it contains.

## ARTICLE

## Improved sensitization efficiency in Er<sup>3+</sup> ions and SnO<sub>2</sub> nanocrystals co-doped silica thin films

Cite this: DOI: 10.1039/x0xx00000x

Xiaowei Zhang,<sup>a,b</sup> Shaobing Lin,<sup>a</sup> Tao Lin,<sup>a,c</sup> Pei Zhang,<sup>a,d</sup> Jun Xu,<sup>\*a</sup> Ling Xu<sup>a</sup> and Kunji Chen<sup>a</sup>

Received 00th January 2012,

Accepted 00th January 2012

DOI: 10.1039/x0xx00000x

[www.rsc.org/](http://www.rsc.org/)

Er<sup>3+</sup> ions and SnO<sub>2</sub> nanocrystals co-doped silica thin films are prepared by improved sol-gel spin-coating method. With increasing annealing temperature, the related 1.54 μm characteristic emission intensity from Er<sup>3+</sup> ions is obviously enhanced by more than two orders of magnitude via SnO<sub>2</sub> nanocrystals size control to boost the sensitization efficiency. Quantitative studies of steady-state spectroscopic data and fluorescence decay curves demonstrate that the related sensitization efficiency via size-tunable nanocrystals is increased from 0.14% to 1.3%. This improved sensitization efficiency is achieved by doping part of Er<sup>3+</sup> ions into the SnO<sub>2</sub> inner sites at high annealing temperature as revealed by high-resolution TEM, X-ray diffraction patterns and elemental mapping technique. Different sensitization mechanisms are also discussed separately according to the selective photoluminescence excitation measurements. All these results have not only explained the greatly improving sensitization efficiency resulting from SnO<sub>2</sub> nanocrystals but also indicated that the development of Er<sup>3+</sup> ions and SnO<sub>2</sub> nanocrystals co-doped silica thin film could be a promising high-performance near-infrared luminous material using broadband UV pumping.

### Introduction

The design and fabrication of a Si-based light source, integrated with optical and electronic components on a single chip, is one of the main challenges in modern optoelectronics<sup>1-3</sup>. Among many emerging metal doped cluster-assembled Si-based materials<sup>4,5</sup>, Erbium (Er<sup>3+</sup>) ion has been considered as the most promising materials for developing Si-based light emitters since the unique 1.54 μm emission corresponded to the minimum absorption window of optical fibers<sup>6,7</sup>. However, due to the sharp absorption peaks of Er<sup>3+</sup> ions, a small absorption cross-section (~2 × 10<sup>-21</sup> cm<sup>2</sup>) limits the realization of highly efficient Er<sup>3+</sup> doped silica based photonic devices<sup>8</sup>. Over the past decade, the sensitizing effect of Si nanocrystals (Si NCs) to surrounding Er<sup>3+</sup> ions offered a promising strategy to improve near-infrared emission intensity of Er<sup>3+</sup> ions<sup>9,10</sup>. Unfortunately, the back energy transfer process from Er<sup>3+</sup> ions to Si NCs inevitably lead to the low near-infrared emission efficiency due to the small band gap of Si NCs<sup>11</sup>.

A proven more effective way is co-doping with wider band gap materials rather than Si NCs, such as zinc oxide nanocrystals (ZnO NCs)<sup>12</sup>, indium oxide nanocrystals (In<sub>2</sub>O<sub>3</sub> NCs)<sup>13</sup> or titanium dioxide (TiO<sub>2</sub> NCs)<sup>14</sup>, taking full advantages of their sensitizing ability to enhance the 1.54 μm emission corresponding to <sup>4</sup>I<sub>13/2</sub> - <sup>4</sup>I<sub>15/2</sub> transition of Er<sup>3+</sup> ions. Generally, these co-doped NCs have relatively large absorption cross-sections to incident UV-light and can effectively improve the density of sensitizing rare-earth ions. In our previous work, the photoluminescence (PL) visible emission intensity at 613 nm from the <sup>5</sup>D<sub>0</sub> - <sup>7</sup>F<sub>2</sub> transition of Eu<sup>3+</sup> ions was enhanced by 20 times<sup>15</sup> and the near-infrared emission intensity of Er<sup>3+</sup> ions was

enhanced by 100 times<sup>16</sup> via co-doping 3 nm In<sub>2</sub>O<sub>3</sub> NCs as sensitizers. Recently, we obtained the size-tunable tin oxide nanocrystals (SnO<sub>2</sub> NCs) in the quantum confinement regime by precisely controlling the Sn concentrations<sup>17</sup>. Co-doping the size-tunable SnO<sub>2</sub> NCs with Er<sup>3+</sup> ions in silica thin films produced an enhancement of Er-related near-infrared emission by three orders of magnitude. However, as for the luminescent efficiency and UV excitation range, the overall performance of Er<sup>3+</sup> ions and wide band gap NCs co-doped silica thin film still remains inferior to that of the best near-infrared light source due to the limited Er<sup>3+</sup> ions' solubility in wide band gap NCs<sup>18</sup>. On the other hand, up to now the fundamental question of whether sensitization mechanism of wide band gap NCs can be tuned by the photonic environment remains under debate<sup>19</sup>. The formation of metal oxide NCs in silica films and the elimination of -OH groups, as the commonest non-radiative recombination centre, are readily influenced by the annealing temperatures<sup>20</sup>. According to the thermo-gravimetric and differential scanning calorimetry (TG/DSC) testing<sup>21</sup>, above 400 °C thermal process is an essential prerequisite for formation of silica films due to the pyrolysis of the residual carbide in TEOS. Here we report the near-infrared emission intensity from Er<sup>3+</sup> ions/SnO<sub>2</sub> NCs co-doped sample is enhanced by more than two orders of magnitude via size control to boost the sensitization efficiency with increasing annealing temperature up to 1000 °C. By combining the steady-state with time-resolved PL spectra excited separately under the 325 nm and 980 nm laser, we quantitatively evaluate the relationship between sensitization efficiency with annealing temperature. According to the high-resolution TEM images, X-ray diffraction patterns and typical

analytical energy dispersive X-ray spectroscopy (EDS) mapping, we confirmed that part of  $\text{Er}^{3+}$  ions doped into the  $\text{SnO}_2$  NCs sites after annealing at 1000 °C, which results in the significant enhancement of sensitization efficiency. We anticipate that our results will be a starting point for the further research, leading to high-performance near-infrared emission of  $\text{Er}^{3+}$  ions for optoelectronics.

## Experimental

$\text{Er}^{3+}$  ions and  $\text{SnO}_2$  NCs co-doped silica thin films were prepared by using sol-gel method and spin-coating technique. A starting solution was obtained by hydrolysis of tetra-ethyl-orthosilicate (TEOS 99.9%, Sigma-Aldrich) in ethanol and de-ionized water. Hydrochloric acid (HCl 0.1mol/L) as a catalyst, was added drop-wise to the starting solution until the pH value of mixture solution reaches close to 2.0. Different amounts of tin tetrachloride ( $\text{SnCl}_4$  98%, Alfa Aesar) and erbium nitride ( $\text{Er}(\text{NO}_3)_3$  99.9%, Sigma-Aldrich) salts were dissolved in the mixture solution to obtain desired concentration. In the present case, the amount of  $\text{Er}^{3+}$  ions added into the precursor solution was fixed at 5% (the molar ratio of Er molecules to Si molecules in the sol precursor, the same as follows) and the amount of Sn was fixed at 20%. Then the precursor was stirred vigorously at 60 °C to complete hydrolysis and gelation was done leaving the sealed container in a thermostatic chamber at 25 °C for one day. Subsequently, the as-prepared gel was spin-coated onto clean Si substrates to form silica thin films by post-annealing treatments at different temperatures for 2 hours in  $\text{N}_2$  flux to activate  $\text{Er}^{3+}$  ions. Simultaneously, the crystalline  $\text{SnO}_2$  nanoparticles were formed during the post-anneal process by hydrolysis of  $\text{SnCl}_4$  salts. All chemical products are used as received without further purification.

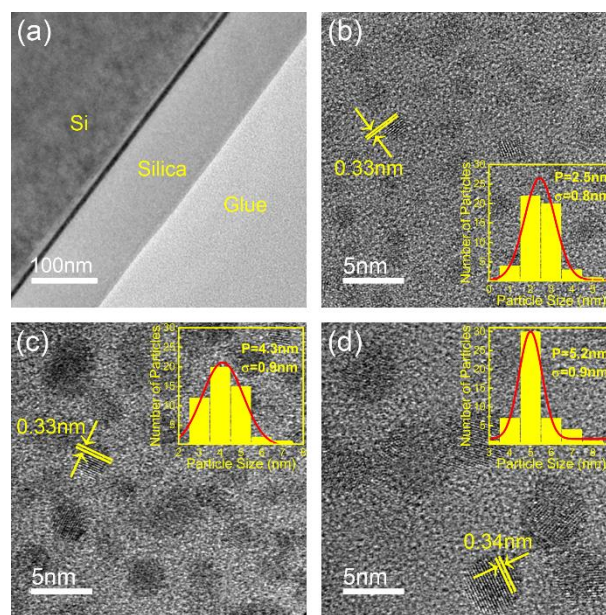
The phase identity and crystalline size of  $\text{SnO}_2$  NCs were determined using a 200 kV energy filtered field emission transmission electron microscopy (FEI, Tecnai-F20). The cross-sectional samples for TEM observation were fabricated by mechanical grinding, polishing and dimpling, followed by Ar-ion milling using a Gatan precision ion polishing system at 4.5 kV with an incident beam angle of 6°. Bonding configurations were studied by Fourier Transform Infrared (FT-IR) spectra (Nicolet, Nexus 870 spectrometer).

Steady-state PL and photoluminescence excitation (PLE) spectra were obtained by using a Horiba Jobin Yvon Fluorolog-3 system equipped with a 325 nm He-Cd laser, 980 nm laser diode and a 450 W Xe lamp as the excitation light sources, separately. A Hamamatsu R 928 photomultiplier tube and a liquid-nitrogen-cooled InGaAs photo-detector with lock-in techniques were used during the measurements. Time-resolved PL spectra were measured by using Edinburgh Photonics FLS 980 fluorescence spectrophotometer based on the time-correlated single photon counting technology. All the spectra were measured at room temperature and corrected for the system response and sample thickness.

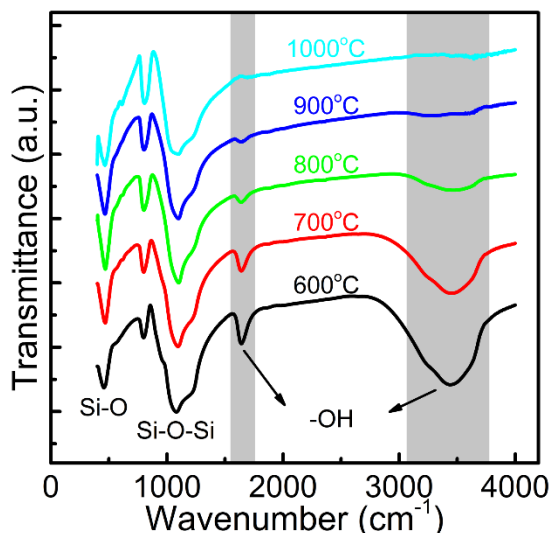
## Result and discussion

Fig. 1(a) is the cross-sectional TEM image and the amorphous silica layer with smooth surface can be identified on Si substrate. Its thickness is around 110 nm. (b) - (d) are the high-resolution TEM images of silica thin films annealed at different temperatures. All these  $\text{SnO}_2$  NCs show clear-cut crystalline features inside the nanoparticles and the measured inter-planar spacing is corresponding to the (110) facets of  $\text{SnO}_2$  NCs tetragonal phase. After annealing at 800 °C, quasi-spherical

crystalline clusters with an average size of 2.5 nm in diameter can be seen discretely embedded in the amorphous silica thin film. The average size of  $\text{SnO}_2$  NCs increases to 5.2 nm with increasing annealing temperature up to 1000 °C. By precisely controlling annealing temperature, we can obtain the size-tunable  $\text{SnO}_2$  NCs with controlled density embedded in amorphous silica thin film. As is well known, luminescent intensity or efficiency is principally governed by the concentration of non-radiative recombination centres mostly influenced by bonding configuration. Thus, we also compare the corresponding FT-IR spectra of amorphous silica thin film after different annealing temperatures from 600 °C to 1000 °C, as presented in Fig. 2. With increasing annealing temperature, the broad -OH groups stretching band centred at 3400  $\text{cm}^{-1}$  gradually diminishes in relative intensity with increasing annealing temperature and is absent after annealing at 900 °C. An identified mechanism for -OH groups' removal is surface desorption of  $\text{H}_2\text{O}$ , which is released upon reaction of surface silanol to form siloxane bridge structures with increasing annealing temperature<sup>10</sup>.



**Fig. 1** (a) shows the cross-sectional TEM image of Si/Silica thin film structure fabricated by spin-coating technique. (b), (c) and (d) are the typical high-resolution TEM images of  $\text{SnO}_2$  NCs doped silica matrix after annealing at 800 °C, 900 °C and 1000 °C, respectively. Insets show the corresponding particle size distribution histograms.



**Fig. 2** FT-IR spectra of SnO<sub>2</sub> NCs doped silica thin films after annealing at different temperatures ranged from 600 °C to 1000 °C.

The characteristic emission of Er<sup>3+</sup> ions at 1.54 μm can be clearly observed in PL spectra both from only Er<sup>3+</sup> ions doped and Er<sup>3+</sup> ions/SnO<sub>2</sub> NCs co-doped samples under the 325 nm excitation. As shown in the inset of Fig. 3, under the 900 °C annealing condition, co-doping SnO<sub>2</sub> NCs with an average size of 4.3 nm into Er<sup>3+</sup> ions embedded silica films produces an enhancement of 1.54 μm emission by more than three orders of magnitude. It can be attributed to the effect sensitization process from SnO<sub>2</sub> NCs with suitable size and density<sup>17</sup>. In order to evaluate the sensitization efficiency from SnO<sub>2</sub> NCs with adjustable size to Er<sup>3+</sup> ions, we measure the changes of PL intensity at 1.54 μm as a function of annealing temperature ranged from 400 °C to 1000 °C for both only Er<sup>3+</sup> ions doped and Er<sup>3+</sup> ions/SnO<sub>2</sub> NCs co-doped films as shown in Fig. 3. For only Er<sup>3+</sup> ions doped silica thin film, the Er-related near-infrared emission appreciably improves with increasing annealing temperature, until it reaches its maximum at 900 °C (red circles in Fig. 3). This increased emission intensity is attributed to elimination of non-radiative recombination centres -OH groups according to the FT-IR results. However, further increasing the annealing temperature to 1000 °C results in decrease of near-infrared PL emission intensity. It can be explained as the concentration quenching process of rare earth ions due to the elimination of -OH groups and aggregation of Er<sup>3+</sup> ions<sup>22</sup>. However, the luminescence behaviour of Er<sup>3+</sup> ions and SnO<sub>2</sub> NCs co-doped samples is quite different (black squares in Fig. 3). The characteristic near-infrared emission intensity of the Er<sup>3+</sup> ions from co-doping samples is obviously enhanced by a factor of ~ 62 with increasing annealing temperature from 400 °C to 1000 °C. This phenomenon indicates a more effective sensitization process from SnO<sub>2</sub> NCs to the nearby Er<sup>3+</sup> ions for co-doped samples, despite of the fact that the density of SnO<sub>2</sub> NCs dramatically decreases with the increased annealing temperature. According to the theory of Förster resonance energy transfer<sup>23</sup>, the sensitization efficiency depends on two main physical parameters that can be grouped as follows: (a) the donor-to-acceptor (SnO<sub>2</sub>-to-Er<sup>3+</sup>) separation distance with an inverse 6<sup>th</sup> power law due to the dipole-dipole coupling mechanism; (b) The spectral overlap integral of the donor emission spectrum and the acceptor absorption spectrum.

For Er<sup>3+</sup> ions/SnO<sub>2</sub> NCs co-doped films, the elimination of -OH groups in silica thin films, revealed by FT-IR results in Fig. 2, leads to the shrinking distance between SnO<sub>2</sub> NCs and Er<sup>3+</sup> ions with increasing annealing temperature. On the other hand, the redshifts of the SnO<sub>2</sub> NCs excitation band due to the increased average size, revealed by high-resolution TEM images in Fig. 1, leads to the slightly enlargement of spectral overlap integral with excitation level of Er<sup>3+</sup> ions. Both shrinking separation distance and enlarged spectral overlaps may contribute to greatly improved sensitization efficiency with increasing annealing temperature for Er<sup>3+</sup> ions/SnO<sub>2</sub> NCs co-doped thin films.

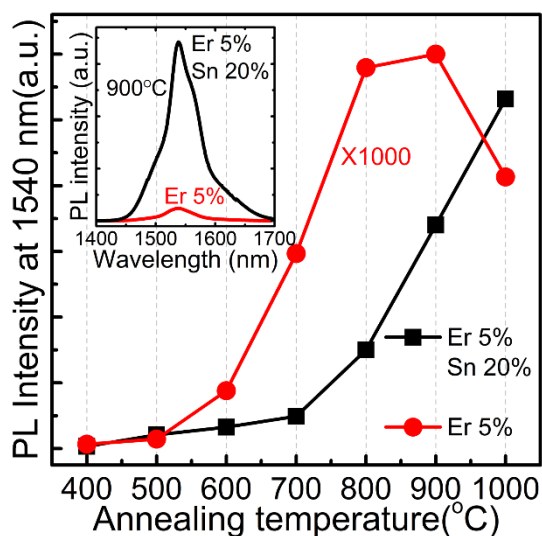


**Fig. 3** The PL intensities for 5% Er<sup>3+</sup> ions and 20% Sn co-doped sample (black squares) and the PL intensities for Sn-free sample (red circles, multiplied by a factor of 1000 to allow the comparison) as a function of annealing temperatures. Inset shows the PL comparison of Sn-free and Er<sup>3+</sup> ions/SnO<sub>2</sub> NCs co-doped silica thin films annealed at 900 °C, respectively. All samples are excited by a 325 nm He-Cd laser.

The PLE spectra are measured by keeping the detected wavelength at 1.54 μm as shown in Fig. 4. These only two sharp PLE peaks at 382 nm and 525 nm correspond to the direct transitions from <sup>4</sup>I<sub>15/2</sub> ground state to <sup>4</sup>G<sub>11/2</sub> and <sup>2</sup>H<sub>11/2</sub> excited states of Er<sup>3+</sup> ions. Interestingly, besides the sharp excitation peaks from the Er<sup>3+</sup> ions' intra-4f transitions, there are two wider and stronger excitation bands located at the position of around 300 nm and 576 nm. The two excitation bands can be attributed to the band gap and the defect-states-energy-level of SnO<sub>2</sub> NCs, respectively. These defect states may originate from the oxygen vacancies produced in the annealing process because the organic species, such as TEOS and ethanol would consume oxygen<sup>24</sup>. The silica layer around the SnO<sub>2</sub> NCs could slow down the oxygen diffusion, which contributes to the recombination of photo-generated carriers trapped by interface states with deep trapped holes, leading to the strong excitation band centred at 576 nm. The redshifts of the excitation band from 293 nm to 322 nm with increasing annealing temperature from 800 °C to 1000 °C can be explained as the enlargement of average sizes of SnO<sub>2</sub> NCs. Meanwhile, according to the effective mass theory<sup>25</sup> and related excitation band positions, we calculate the average size of SnO<sub>2</sub> NCs and demonstrate that the results are remarkably consistent with the TEM

observations (see supplemental discussion 1 and Table 1S<sup>†</sup> in the supporting information). It is found that the average sizes of SnO<sub>2</sub> NCs increase from 2.92 nm to 5.12 nm with increasing annealing temperature from 800 °C to 1000 °C. Herein, we infer two kind of possible channels for the Er<sup>3+</sup> ions excitations based on the above measurement results. The several sharp excitation peaks indicate a direct excitation of the Er<sup>3+</sup> ions from the ground state to the excited ones while the two wide excitation bands indicate an indirect sensitization mechanism through defect-states-energy-level to valence band (VB) transition and band-to-band transition of the SnO<sub>2</sub> NCs with specific size and density. Both sensitization processes may contribute to significant improvement of sensitization efficiency.

As shown in Fig.5, one part of UV incident photons are absorbed by the SnO<sub>2</sub> NCs and promotes the electrons through band-to-band transition. Due to the slightly spectral mismatch between the valence band of SnO<sub>2</sub> NCs and the excitation level of Er<sup>3+</sup> ions, most of the photo-excited electrons are subsequently trapped by the defect states through the non-radiative decay process while a tiny fraction of energy is transferred to surrounding Er<sup>3+</sup> ions via non-radiative recombination process. Simultaneously, the other part of UV excitation light is absorbed by the SnO<sub>2</sub> NCs through promoting the electrons from valence band to defect-states-energy-level transition. Because of the suitable spectral overlap between the defect-states-energy-level of SnO<sub>2</sub> NCs and the <sup>2</sup>H<sub>11/2</sub> excitation level of Er<sup>3+</sup> ions, more effective sensitization process can occur according to the theory of Förster resonance energy transfer<sup>23</sup>, which induces the Er<sup>3+</sup> ions-related excited electrons jumping from the ground state to the excited ones and then generates the high-performance near-infrared emission.

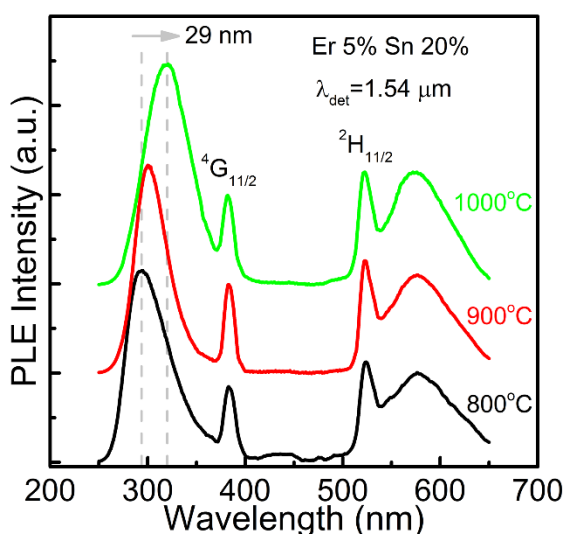


**Fig. 4** PLE spectra of co-doped samples with different annealing temperature from 800 °C to 1000 °C by detecting emission wavelength at 1.54 μm. Inset shows the possible mechanisms for Er<sup>3+</sup> ions sensitization process by size-tunable SnO<sub>2</sub> NCs.

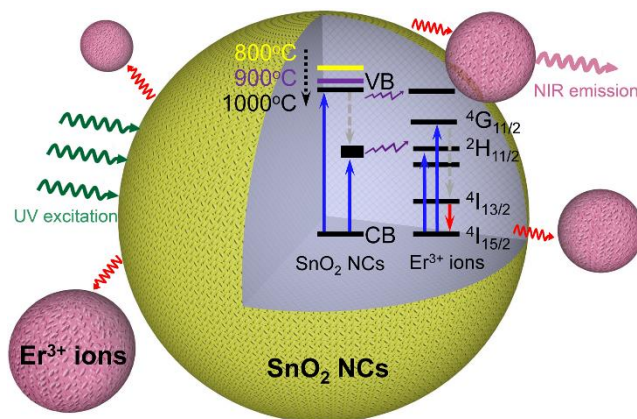


**Fig. 5** General depiction of sensitization mechanism via size-tunable SnO<sub>2</sub> NCs under UV excitation.

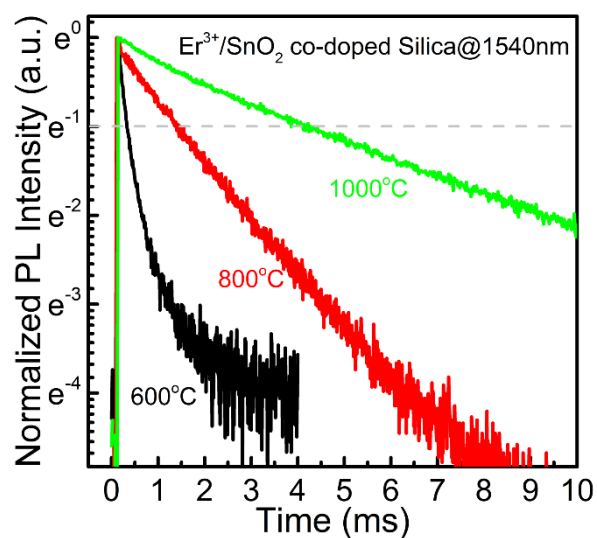


**Fig. 6** Luminescence decay curves from time-resolved PL measurements of the Er<sup>3+</sup> ions characteristic emission at 1.54 μm with different annealing temperatures under 300 nm excitation.

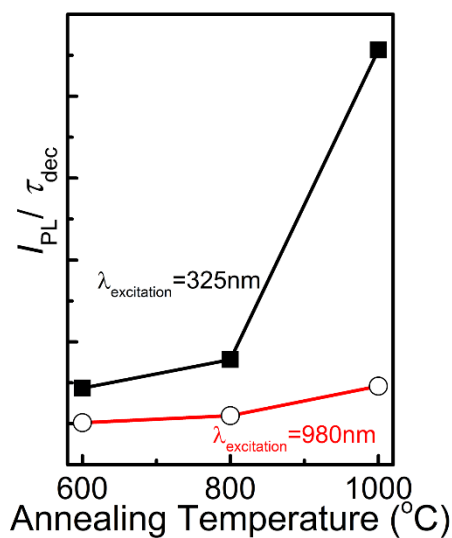


**Fig. 7** illustrates the  $(I_{\text{PL}}/\tau_{\text{dec}})$  vs.  $t$  plots under the different excited wavelength, 325 nm and 980 nm, respectively.

To further evaluate the sensitization mechanism in co-doped samples, the time-resolved PL spectra are measured for samples after annealing at various temperatures as shown in Fig. 6. The mean decay lifetimes of the emission at 1.54  $\mu\text{m}$  are obtained from the following equation,

$$\tau_{\text{dec}} = \int I(t) \times dt / I_{\text{max}} \quad (1)$$

where  $I(t)$  is the time-dependent PL intensity at 1.54  $\mu\text{m}$  and  $I_{\text{max}}$  is the maximal PL intensity at the initial time. Clearly, the lifetime of 1.54  $\mu\text{m}$  emission ( $\tau_{\text{dec}}$ ) shows a monotonically increased from 0.36 ms to 4.15 ms, as annealing temperature increases from 600  $^{\circ}\text{C}$  to 1000  $^{\circ}\text{C}$ . The value obtained here are similar to those obtained before in samples with similar Sn excess<sup>26</sup>. The lengthening of the PL lifetime that results from increasing annealing temperature is related to the elimination of -OH groups on the SnO<sub>2</sub> NCs surface. In a linear excitation regime, the PL intensity can be obtained from the following equation,

$$I_{\text{PL}} \sim \varphi \sigma_{\text{Er}} N_{\text{Er,act}} \frac{\tau_{\text{dec}}}{\tau_{\text{rad}}} \quad (2)$$

where  $\varphi$  is the photon flux,  $\sigma_{\text{Er}}$  is the effective excitation cross-section of activator Er<sup>3+</sup> ions and  $N_{\text{Er,act}}$  is the density of activated Er<sup>3+</sup> ions.  $N_{\text{Er,act}}$  includes two parts, activated Er<sup>3+</sup> ions density by direct optically excitation and other one by sensitization of SnO<sub>2</sub> NCs.  $\tau_{\text{dec}}$  is the decay time and  $\tau_{\text{rad}}$  is the radiative lifetime. After a simple transformation, Eq. 2 can be expressed as follow,

$$N_{\text{Er,act}} \sim \frac{\tau_{\text{rad}} I_{\text{PL}}}{\varphi \sigma_{\text{Er}} \tau_{\text{dec}}} \quad (3)$$

Assuming that  $\sigma_{\text{Er}}$  and  $\tau_{\text{rad}}$  are annealing temperature independent<sup>27</sup>, the density of activated Er<sup>3+</sup> ions should be proportional to the ratio of PL integral intensity to the corresponding decay time. Fig. 7 shows the results of  $I_{\text{PL}}/\tau_{\text{dec}}$  for co-doped samples after annealing at different temperatures under the 980 nm and 325 nm laser excitation, respectively. Note that the 980 nm line corresponds to the transition of Er<sup>3+</sup> ions from <sup>4</sup>I<sub>15/2</sub> - <sup>4</sup>I<sub>11/2</sub> and cannot be absorbed by SnO<sub>2</sub> NCs in silica thin films. That is to say, we can exclude the sensitizing effect of SnO<sub>2</sub> NCs on Er<sup>3+</sup> ions by using a 980 nm laser as an excitation light source. In this case,  $I_{\text{PL}}$  can be expressed as Eq. 2 and  $N_{\text{Er,act}}$  should be modified to the density of Er<sup>3+</sup> ions by direct optically excitation. Thus the ratio  $I_{\text{PL}}/\tau_{\text{dec}}$  gives the evolution information on  $N_{\text{Er,act}}$  for samples under various annealing temperatures. The  $I_{\text{PL}}/\tau_{\text{dec}}$  ratio is almost flat under the 980 nm laser excitation, which indicates this observed change in the PL intensity can be almost fully ascribed to the variety of the decay time and with no effect on  $N_{\text{Er,act}}$ . However, the  $I_{\text{PL}}/\tau_{\text{dec}}$  ratio under 325 nm laser excitation is higher than that under the 980 nm laser excitation. As discussed before, the SnO<sub>2</sub> NCs in silica thin films can act as sensitizers, which absorb the incident photons and then excite the surrounding Er<sup>3+</sup> ions via indirect sensitization process induced by defect-states-energy-level to value band transition and band-to-band transition. The increase value of  $I_{\text{PL}}/\tau_{\text{dec}}$  suggests that the more Er<sup>3+</sup> ions can be activated in co-doped samples under 325 nm laser excitation, which can be attributed to the effective sensitizing effect of SnO<sub>2</sub> NCs. For estimating the sensitization efficiency of SnO<sub>2</sub> NCs in co-doped samples, we calculate the density of activated Er<sup>3+</sup> ions based on the method reported by

B. Garrido et al.<sup>28</sup> and define the sensitization efficiency ( $\eta$ ) as the fraction of the number of sensitizing Er<sup>3+</sup> ions over the total Er<sup>3+</sup> ions number in silica thin films.

$$\eta = \frac{N_{\text{Er,325nm}} - N_{\text{Er,980nm}}}{N_{\text{Er}}} \times 100\% \quad (4)$$

For the co-doped samples, the value of  $\eta$  increases from 0.14% to 1.3% with increasing annealing temperature from 600  $^{\circ}\text{C}$  to 1000  $^{\circ}\text{C}$ . It is explained as shrinking separation distance and enlarged spectral overlaps. Another possibility is the fact that Er<sup>3+</sup> ion enter into the SnO<sub>2</sub> NCs, which induces the significant improvement of sensitization efficiency due to the occurrence of Dexter Energy Transfer (DET) process, or charge exchange mechanism instead of Förster Resonance Energy Transfer (FRET) process. It is also worth noting that the phonon energy of SnO<sub>2</sub> NCs is quite small ( $\sim 630 \text{ cm}^{-1}$ )<sup>29</sup>, which is lower than the one of amorphous silica ( $\sim 1000 \text{ cm}^{-1}$ )<sup>30</sup>. Consequently, the non-radiative recombination rate corresponding to phonon-assisted energy transfer to host vibrations is much lower if Er<sup>3+</sup> ions are partially partitioned into SnO<sub>2</sub> sites. Therefore, the sensitization efficiency is improved from 0.14% to 1.3% in co-doped samples with increasing annealing temperature to 1000  $^{\circ}\text{C}$ , which lead to the significant enhancement of near-infrared emission of Er<sup>3+</sup> ions.

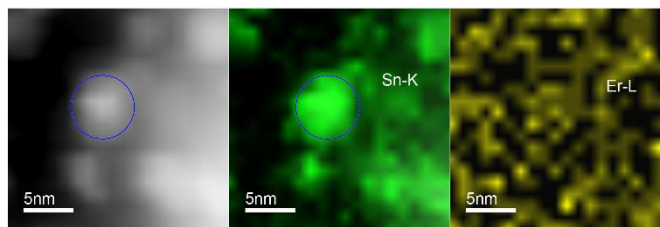


**Fig. 8** (a) the cross-sectional dark-field STEM image. (b) and (c) Elemental mapping of the same region, indicating spatial distribution of Sn (green) and Er (yellow), respectively.

Our present results indicate that parts of Er<sup>3+</sup> ions remain in the amorphous silica matrix and the others are trapped in the SnO<sub>2</sub> NCs, similar to that of Eu<sup>3+</sup> in SnO<sub>2</sub> NCs reported before<sup>31</sup>. Generally, the Er<sup>3+</sup> ions are very hard to dissolve in Sn<sup>4+</sup> sites due to the large radius mismatch and the charge imbalance (0.088 nm for Er<sup>3+</sup> ions, 0.071 nm for Sn<sup>4+</sup> ions). However, it has been reported that the Er<sup>3+</sup> ions were successfully doped into SnO<sub>2</sub> NCs with Er<sup>3+</sup> doping concentration of 0.043 at.%<sup>32</sup>. Calculated from the high-resolution TEM images in Fig. 1 (b)-(c), the inter-planar spacing of the (110) plane increases from 0.33 nm to 0.34 nm due to the lattice expansion. This slight increase reveals the fact that a small fraction of Er<sup>3+</sup> ions get incorporated at the interstitial sites though most of them could be segregated to the surface of the SnO<sub>2</sub> NCs. The X-ray diffraction patterns also confirm the formation of SnO<sub>2</sub> NCs and doping of Er<sup>3+</sup> ions due to the slight shifting (see supplemental discussion 2 and Fig. 1S<sup>†</sup> in the supporting information). We also use the TEM elemental mapping technique to characterize the element distribution. As seen in Fig. 8 (a)-(c), it is revealed contrast indicative of variations in the chemical composition. STEM energy-dispersive EDS mapping of the same nanocrystals region confirms the formation of SnO<sub>2</sub> NCs and indicate parts of Er<sup>3+</sup> ions remain in the amorphous silica matrix, and the others are trapped in the SnO<sub>2</sub> NCs after thermal treatments at 1000  $^{\circ}\text{C}$ . Though the present results need to further investigation, we believe that the partial incorporation of Er<sup>3+</sup> ions into the SnO<sub>2</sub> sites plays a

significant role in the enhancement of sensitization efficiency in co-doped samples, especially for 1000 °C annealed samples.

## Conclusion

In summary, amorphous silica thin films uniformly co-doped with size-tunable SnO<sub>2</sub> NCs and Er<sup>3+</sup> ions have been fabricated via a facile sol-gel method and spin-coating technique. With increasing annealing temperature, the characteristic emission of 1.54 μm from Er<sup>3+</sup> ions is obviously enhanced by more than two orders of magnitude due to the high-efficiency sensitization of SnO<sub>2</sub> NCs. PLE results indicate that the UV incident photons are absorbed by SnO<sub>2</sub> NCs through band-to-band transition and defect-states-energy-level to value band transition when Er<sup>3+</sup> ions sensitization process occurs. The related sensitization efficiency is increased from 0.14% to 1.3% based on quantitative studies of steady-state and time-resolved spectroscopic data. Furthermore, high-resolution TEM images, X-ray diffraction patterns and EDS mapping results offer the direct experimental evidences for the partial incorporation of Er<sup>3+</sup> ions into the SnO<sub>2</sub> sites, which explains the greatly improving sensitization efficiency via size-tunable Sn NCs. The development of high sensitization efficiency of SnO<sub>2</sub> NCs could open up potentials in improving spectral response of photovoltaic devices, boosting outputs of optical amplifiers or phosphors, and increasing photon up-conversion efficiency of bio-imaging. We envision that these and other applications may benefit from the improving Er<sup>3+</sup> ions sensitization efficiency.

## Acknowledgements

This work is supported by "973 program" (2013CB632101), NSFC (11274155) and PAPD. One of the authors X. Zhang also expresses thanks to the State-Sponsored Study Abroad Programs of China Scholarship Council (201406190080) and Scientific Research Foundation of Graduate School of Nanjing University (2014CL01).

## Notes and references

<sup>a</sup>National Laboratory of Solid State Microstructures, Department of Electronic Science and Engineering and Collaborative Innovation Centre of Advanced Microstructures, Nanjing University, Nanjing, 210093, China. E-mail: [junxu@nju.edu.cn](mailto:junxu@nju.edu.cn); Fax: +86-25-83594836; Tel: +86-25-83595535.

<sup>b</sup>Materials Sciences Division, Lawrence Berkeley National Laboratory, Berkeley, California, 94720, USA. E-mail: [xiaoweizhang@lbl.gov](mailto:xiaoweizhang@lbl.gov)

<sup>c</sup>Department of Physics, Guangxi University, Nanning, 530004, China.

<sup>d</sup>Henan Key Lab of Information-based Electrical Appliances, Department of Electrical and Information Engineering, Zhengzhou University of Light Industry, Zhengzhou, 450002, China.

†Electronic Supplementary Information (ESI) available. See DOI: 10.1039/b000000x/

- W. L. Ng, M. A. Lourenco, R. M. Gwilliam, S. Ledain, G. Shao and K. P. Homewood, *Nature*, 2001, **410**, 192.
- D. Liang and J. E. Bowers, *Nat. Photonics*, 2010, **4**, 511.
- C. H. Cho, C. O. Aspetti, J. Park and R. Agarwal, *Nat. Photonics*, 2013, **7**, 285.
- G. K. Gueorguiev, S. Stafstrom and L. Hultman, *Chem. Phys. Lett.*, 2008, **458**, 170.
- M. J. T. Oliverira, P. V. C. Medeiros, J. R. F. Sousa, F. Nogueira and G. K. Gueorguiev, *J. Phys. Chem. C*, 2014, **118**, 11377.
- P. J. Mears, L. Reekie, I. M. Jauncey and D. N. Payne, *Electron. Lett.*, 1987, **23**, 1026.
- X. Zhang, T. Lin, X. Jiang, J. Xu, J. Liu, L. Xu and K. Chen, *Chin. Opt. Lett.*, 2012, **10**, 091603.
- F. Wang and X. G. Liu, *Chem. Soc. Rev.*, 2009, **38**, 976.
- M. Fujii, M. Yoshida, Y. Kanzawa, S. Hayashi and K. Yamamoto, *Appl. Phys. Lett.*, 1997, **71**, 1198.
- G. Franzo, E. Pecora and F. Priolo, *Appl. Phys. Lett.*, 2007, **90**, 183102.
- J. M. Ramirez1, S. Cuff, Y. Berencen, C. Labbe and B. Garrido, *J. Appl. Phys.*, 2014, **116**, 083103.
- F. Xiao, R. Chen, Y. Q. Shen, Z. L. Dong, H. H. Wang, Q. Y. Zhang and H. D. Sun, *J. Phys. Chem. C*, 2012, **116**, 13458.
- Y. L. Yu, D. Q. Chen, Y. S. Wang, P. Huang, F. Y. Weng and M. T. Niu, *Phys. Chem. Chem. Phys.*, 2009, **11**, 8774.
- C. Y. Fu, J. S. Liao, W. Q. Luo, R. F. Li and X. Y. Chen, *Opt. Lett.*, 2008, **33**, 953.
- N. Wan, J. Xu, T. Lin, X. G. Zhang and L. Xu, *Appl. Phys. Lett.*, 2008, **92**, 201109.
- T. Lin, X. W. Zhang, J. Xu, M. Swihart, L. Xu and K. J. Chen, *Appl. Phys. Lett.*, 2013, **103**, 181906.
- X. W. Zhang, T. Lin, P. Zhang, J. Xu, S. B. Lin, L. Xu and K. J. Chen, *Opt. Express*, 2014, **22**, 369.
- X. M. Li, F. Zhang and D. Y. Zhao, *Chem. Soc. Rev.*, 2015.
- F. T. Rabouw, S. A. Hartog, T. Senden and A. Meijerink, *Nat. Commun.*, 2014, **5**, 3610.
- T. T. Van, S. Turrell, B. Capoen, L. V. Hieu, M. Ferrari, D. Ristic, L. Boussekey and C. Kinowski, *J. Mater. Sci.*, 2014, **49**, 8226.
- N. Wan, T. Lin, J. Xu, L. Xu and K. J. Chen, *Nanotechnology*, 2008, **19**, 095709.
- M. K. G. Jayakumar, K. Huang and Y. Zhang, *Nanoscale*, 2014, **6**, 8439.
- R. M. Clegg, *Curr. Opin. Biotech.*, 1995, **6**, 103.
- J. Castillo, V. D. Rodriguez, A. C. Yanes and J. M. Ramos, *J. Nanopart. Res.*, 2008, **10**, 499.
- L. Brus, *J. Phys. Chem.*, 1986, **90**, 2555.
- S. Brovelli, N. Chiodini, F. Meinardi, A. Monguzzi, A. Lauria, R. Lorenzi, B. Vodopivec, M. C. Mozzati and A. Paleari, *Phys. Rev. B*, 2009, **79**, 153108.
- K. Hijazi, R. Rizk, J. Cardin, L. Khomenkova and F. Gourbilleau, *J. Appl. Phys.*, 2004, **95**, 3717.
- B. Garrido, C. Garc ía, S. Y. Seo, P. Pellegrino, D. Navarrourios, N. Daldosso, L. Pavesi, F. Gourbilleau and R. Rizk, *Phys. Rev. B*, 2007, **76**, 245308.
- N. Chiodini, A. Paleari, G. Brambilla and E. R. Taylor, *Appl. Phys. Lett.*, 2002, **80**, 4449.
- W. J. Miniscalco, *J. Lightwave. Technol.*, 1991, **9**, 234.
- X. W. Zhang, T. Lin, J. Xu, L. Xu and K. J. Chen, *Chin. Phys. B*, 2012, **21**, 018101.
- J. T. Kong, H. M. Zhu, R. F. Li, W. Q. Luo and X. Y. Chen, *Opt. Lett.*, 2009, **34**, 1873.